https://dx.doi.org/10.4314/ijs.v25i1.10

KINETICS AND EQUILIBRIUM ADSORPTION STUDIES OF CHROMIUM (VI) AND IRON (III) FROM AQUEOUS SOLUTION SYSTEMS USING HYDROXYAPATITE, ACTIVATED CARBON AND THEIR COMPOSITES

Adegoke, H. I.*, Ashola, M. O. and Audu, M. F.
Department of Chemistry, University of Ilorin, P.M.B. 1515, Ilorin, Nigeria.
*Corresponding Author's Email: adegoke.hi@unilorin.edu.ng
(Received: 21st December, 2022; Accepted: 14th April, 2023)

ABSTRACT

Industrial effluents have become an environmental issue harming the ecosystem, remediation of these effluents is critical in order to mitigate some of this issue. Three adsorbents, activated carbon from sugarcane bagasse (ASB), hydroxyapatite (HAP), and their composites (ncpA), were prepared for the adsorption of Cr (VI) and Fe (III) from wastewater in this work. The hydroxyapatite was synthesized using the wet precipitation method, and the activated carbon was derived from sugarcane bagasse, resulting in a composite with a hydroxyapatite to activated carbon ratio of 1:1. The adsorbents surface and chemical properties were determined by Fourier transform infrared spectroscopy (FT-IR), scanning electron microscopy (SEM), Brunauer-Emmett-Teller (BET), and X-ray diffraction (XRD). The BET surface areas were 1.34 ± 0.04 m^2/g and 26.4 ± 0.4 m^2g^{-1} for HAP and ASB respectively. The influence of initial concentration of metal ions, adsorbent dosage, pH, contact time and temperature on the adsorption process were investigated. Two isotherm models and different kinetic models were used in fitting the experimental data. The adsorption of Cr (VI) and Fe (III) fitted well into the Langmuir isotherm model with maximum monolayer adsorption capacities of 19.92 mg/g, 16.69 mg/g and 10.33 mg/g respectively for Cr (VI) and 113.64 mg/g, 113.64 mg/g and 107.54 mg/g respectively for Fe (III) removal onto HAP, ASB and ncpA respectively. The pseudo-second-order model that best suited the kinetic data was chemisorption-controlled, and this is referred to as the mechanism of the adsorption. Sum of square error (SSE) and non-linear chi-square (χ^2) were used to further validate the mechanism.

Keywords: Adsorption, Kinetics, Equilibrium, Hydroxyapatite, Sugar cane bagasse.

INTRODUCTION

Rapid urbanization and industrialization had engendered the discharge of harmful heavy metals into the aquatic system. Chemical elements with densities more than 5 g/cm^3 are referred to be heavy metals. Considering their toxicity and long-lasting negative impacts on human health, they are among the most dangerous water contaminants (Mortazavian *et al.*, 2018). In a consequence to preserve the ecosystem from harmful contaminants, it is crucial to remove them from water system. The heavy metals of interest in this study are chromium [Cr (VI)] and iron [Fe (III)]. Chromium is used in many industrial processes, including electroplating, leather tanning, the fabric industry, and the production of dyes and pigments (Jaishankar, 2014). Because of its ability to induce cancer in living things, chromium is regarded as one of the most dangerous inorganic pollutant (Ali *et al.*, 2021).

The oxidation states of chromium in an aqueous solution are trivalent [Cr (III)] and hexavalent [Cr (VI)]. Cr (III) exhibits reduced toxicity and less mobility as compared to Cr (VI) (Kantar *et al.*, 2015). The World Health Organization (WHO) revealed that wastewater from industrial effluents has an acceptable Cr (VI) concentration limit of 0.5 mg/L and drinking water limit of 0.05 mg/L (WHO, 2017).

One of the most significant metals whose concentration must be kept below the permitted concentration limit in an aquatic environment is iron. Many industries, including the paint, automotive, aerospace, and steel industries discharge wastewaters that have obscenely high iron concentrations chromium (Mahanna *et al.*, 2021). Haemochromatosis, diabetes mellitus, liver cancer, cirrhosis, oliguria, and two phases shock are all conditions that can result from having too much iron in the body (Li *et al.*, 2016; Dim *et al.*, 2021). Hence, it is crucial to treat water and wastewater containing Fe (III) ions to a level below the permissible limit of 0.3 mg/L (WHO, 2017).

The elimination of heavy metals from water or

simulated solutions is of vital environmental concern. Numerous technological methods have been employed to eliminate heavy metals and organic pollutants from effluent, examples include adsorption (Gusain, 2020), electrochemical methods (Nur-E-Alam, 2020), chemical precipitation (Minas *et al.*, 2017), membrane separation (Kozlowski and Walkowiak, 2002), and ion exchange (Ren *et al.*, 2020). Surface adsorption method has emerged as the most effective, financially feasible, environmentally friendly, and technologically promising process (Aldawsari *et al.*, 2021).

Lately, biologically derived substances including hydroxyapatite and activated carbon have been investigated as effective adsorbents to eliminate hazardous inorganic and organic pollutants from effluents (Kousalya *et al.*, 2010). The calcium phosphate mineral of hydroxyapatite (HA), $Ca_{10}(PO_4)_6(OH)_2$, is a naturally occurring member of the apatite family ($A_{10}(BO_4)X_2$) (Khandelwal and Prakash, 2016).

The characteristic properties of hydroxyapatite include biocompatibility, bioactivity, nontoxicity, non-inflammatory, and non-immunogenicity (Mohamed *et al.*, 2011). Unmixed or uncontaminated hydroxyapatite is thermally stable at 1200 °C (Narayan *et al.*, 2004). These properties, along with its high surface assimilation properties, low solubility in water (K_{sp} less than 10^{-40}), high strength under heating and reduction-oxidation environments, affordability and obtainability, made it a very good material for the treatment of pollutants (Khandelwal and Prakash, 2016).

Wet precipitation method (Prabakaran *et al.*, 2005), hydrothermal technique (Agrawal *et al.*, 2011), low temperature synthesis (Sasikumar and Vijayaraghavan, 2006), solid state reaction and sol-gel technique (Raihana *et al.*, 2008) are a few of the conventional methods utilized in the synthesis of hydroxyapatite.

Due to the special characteristics of hydroxyapatite, researchers have worked to advance its use in wastewater remediation since combining it with appropriate supporting materials such as activated carbon, chitosan, graphene, and polymeric materials tend to enhance its adsorption ability. Yet, the excessive Hap particle aggregation could restrict the composite's ability to adsorb contaminants (Li *et al.*, 2019). In a recent work, Nasrellah *et al.* (2022) prepared thin coating of some adsorbents such as chitosan, hydroxyapatite and montmorillonite for effective removal of Cr (VI) from aqueous solutions.

In this investigation, activated carbon obtained from sugarcane baggase, hydroxyapatite and their composites were prepared and their adsorption properties for removing Cr (VI) and Fe (III) ions from aqueous solutions was evaluated.

MATERIALS AND METHODS

Materials

Analytical grade reagents were used in this study without further purification. These include, diammonium hydrogen phosphate $(NH_4)_2HPO_4$, calcium hydroxide $[Ca(OH)_2]$, orthophosphoric acid (H_3PO_4), ammonium hydroxide (NH_4OH), sodium chloride (NaCl), calcium nitrate tetrahydrate $[Ca(NO_3)_2.4H_2O]$, sodium hydroxide (NaOH) and hydrochloric acid (HCl). Stock solutions of Cr (VI) and Fe (III) ions were made using potassium dichromate $(K_2Cr_2O_7)$, iron (III) nitrate nonahydrate $[Fe(NO_3)_3.9H_2O]$ and deionized water.

Carbonization of Sugarcane Bagasse

The sugarcane bagasse was collected after juicing out the liquid in sugarcane. Deionized water was used to thoroughly wash the raw sugarcane bagasse, removing any trapped and ligneous contaminants. In order to remove any contaminants, the bagasse was washed many times with deionized water. A consistent weight was attained after drying the purified bagasse in an oven for 24 h at 105 °C. The dried sugarcane bagasse was pyrolyzed in a muffle furnace set to 400 °C for 1 h. The prepared activated carbon was ground, sieved, and labeled as ASB.

Synthesis of Hydroxyapatite

Hydroxyapatite (HAP) suspension was prepared by wet chemical precipitation method (Prabakaran *et al.*, 2005). The pH of the solution was monitored during the precipitation reaction, and acid was added to calcium hydroxide solution. For the orthophosphoric acid and calcium hydroxide,

the reactant concentrations are 0.5 M and 0.3 M, respectively. H_3PO_4 solution was applied dropwise for 3 h, over the alkaline solution based on $Ca(OH)_2$, with vigorous stirring, to produce a hydroxyapatite slurry. To produce a stoichiometric hydroxyapatite (Ca/P = 1.67), the pH was maintained at 9.5–10 during the addition process using concentrated aqueous ammonia solution, NH_4OH. The reaction mixture was aged at room temperature for 48 hours following the final addition. Dialysis was used to wash the precipitate, and a millipore glass membrane vacuum filtration system was used to filter it. The filtered cake was ground to a powder in a mortar and pestle after oven drying at 130 °C for 24 h.

Preparation of Nanocomposites

The composites of HAP and ASB were prepared in the ratio of 1:1. The activated carbon from sugarcane bagasse (ASB) was added to 0.1 M HCl and stirred for about 1 h. After adding the hydroxyapatite (HAP), it was agitated for a further 30 min. The mixtures were filtered and washed. The sample was labeled HAP.

Determination of Physicochemical Properties of Activated Carbon, Hydroxyapatite and their Composites

The percentage yield, moisture content, ash content, percentage fixed carbon (mg/g), and iodine number (mg/g) of ASB, HAP, and ncpA were all determined using standard methods. The pH drift method was used to determine pH of point of zero charge (pH_{pzc}) of the adsorbents (Bello *et al*., 2020). 25 mL Portions of prepared 0.01 M NaCl solution was transferred into 250 mL conical flasks. The pH of the solutions was adjusted to a range of 2 to 10 with 0.5 M of NaOH and 0.5 M HCl. The electrolyte solution's pH was noted as being $pH_{initial}$. In the conical flasks, 20 mL of the solution and 0.5 g of the adsorbents were added, sealed, and allowed to equilibrate for 24 h. The final pH (pH_{final}) was measured, and a pH change plot ($pH_{final} - pH_{initial}$) vs $pH_{initial}$ was drawn. The pH_{pzc} was determined by taking the intersection of the graph of pH change and $pH_{initial}$ (Nasiruddin and Sarwar, 2007).

Spectroscopic Characterization of Adsorbents

The following spectroscopic techniques were employed in the surface characterization of the prepared adsorbents: X-ray diffraction (XRD) Spectroscopy Philips APD-3720 model diffractometer with Cu Kα radiation, operated at 40 kV, 40 mA, scanning electron microscopy (SEM) SEM QUANTA 250 model with an acceleration voltage of 20.00 kV, Brunauer-Emmett-Teller (BET) BIT and BYTE (BET 225) model and Fourier Transform Infrared Spectroscopy (FTIR) Bruker Alpha FTIR spectrometer. The adsorbent's surface functional groups were determined using FT-IR. SEM was used to analyze the surface morphology of the adsorbents. The specific surface area of the adsorbents was determined using BET and XRD was utilized to help identify the crystal phases and degree of crystallinity of HAP.

Adsorption Experiments

To prepare the stock solution of Cr (VI), 2.826 g of $K_2Cr_2O_7$ (Analytical grade) was dissolved in 1000 mL of deionized water to get 1000 mg/L of Cr (VI). To obtain a 1000 mg/L solution for the stock solution of Fe (III), 7.23 g of $Fe(NO_3)_3.9H_2O$ (Analytical grade) was dissolved in 1000 mL of deionized water. All reagents used were purchased from Sigma-Aldrich. On a mechanical shaker, batch adsorption experiment was carried out. 20 mL Portions of the aqueous solutions of Cr (VI) and Fe (III) were placed in a 100 mL conical flask, and were then in contact with a measured mass of the adsorbents (HAP, ASB and ncpA). 0.5 M NaOH and 0.5 M HCl were used to adjust the pH of the solutions. For two hours, the suspension was shaken at a steady speed of 150 rpm. It was examined based on how different factors, including the initial concentration of metal ions (5–100 mg/L), adsorbent dosage (10 –150 mg), pH (1-8), contact time (30–240 min), and temperature (20–67 °C), affected the adsorption process. The supernatant solutions were removed once the allotted amount of time for adsorption had passed, and were then filtered using Whatman filter paper. Atomic absorption spectrometer (AAS) was used to measure the amounts of the remaining metal ions. The expression in Eq. 1 was used to estimate the quantity of metal ions adsorbed.

$$q_e = \frac{C_o - C_e}{m} \times V \quad (1)$$

Where V is the volume of the adsorbate (L), m (mg) is the mass of the adsorbent employed, q_e (mg/g) is the quantity of Cr (VI)/Fe (III) adsorbed at equilibrium, C_o (mg/L) is the initial concentration of Cr (VI)/Fe (III), C_e (mg/L) is the equilibrium concentration of Cr (VI)/Fe (III).

RESULTS AND DISCUSSION

Physico-chemical Characterization of Adsorbents

The results of some of the physicochemical characteristics for HAP and ASB are displayed in Table 1. HAP and ASB both have pH values of 6.83 and 7.8, respectively. As observed by other researchers, this was within the pH range suitable for adsorption procedures (Ekpete and Horsfall, 2011; Dada *et al.*, 2020). As previously reported, the pH of the produced hydroxyapatite (HAP) was determined to be 7.9 whereas that of the activated carbon from sugarcane bagasse (ASB) was 6.8 (Skwarek *et al.*, 2014). In comparison to reported yields of 66.5% (Eletta *et al.*, 2021) and 46.08% (Sahu *et al.*, 2010) obtained from other sources, the percentage yield of the activated carbon obtained was 98.2%. This shows that sugarcane bagasse is a good starting material for the preparation of activated carbon. Moisture content, a measurement of how much water the activated carbon retains, was found to be 11% for ASB. This value is lower than that reported elsewhere, 18.3% (Bello *et al.*, 2021). An activated carbon's ash content, which rises with an increase in carbonization temperature, reveals how many inorganic components are present in the material (Adebayo *et al.*, 2015). The percentage ash content of ASB was 18%, lower than that of activated carbon obtained from stem bark of Daniellia oliveri tree (Adebayo *et al.*, 2020) and higher than those of the Ziziphus jujube core activated carbon (Labied *et al.*, 2018) and date seed (Mane *et al.*, 2005). The adsorbent's level of activity is measured by its iodine number; the higher the iodine number, the greater the degree of activation and the formation of the micropores (Baseri *et al.*, 2012). The prepared ASB has an iodine number of 1116.72 mg/g, which is greater than the 600 mg/g obtained for activated carbon from olive stone (Aziz *et al.*, 2009) and 798 mg/g from Thevetia peruviana activated carbon (Baseri *et al.*, 2012).

Table 1: Physicochemical properties of hydroxyapatatite and activated carbon of sugar cane baggase.

Parameter	HAP	ASB	ASB (other studies)
pH	7.8	6.83	6.8 (Skwarek *et al.*, 2014)
pH_{pzc}	7.9	6.8	7.4 (Farahani *et al.*, 2011)
Colour	White	Black	black (Farahani *et al.*, 2011)
Surface area	1.34±0.04	26.4±0.4	829 (Luana *et al.*, 2017)
% yield	98.2%	89%	66.5% (Eletta *et al.*, 2021)
Moisture content	------	11%	15 % (Farahani *et al.*, 2011)
Ash content	------	18%	-
Iodine number	------	1116.72	647.94 (Chen *et al.,* 2012)

Functional Group Analysis of Activated Carbon of Sugarcane Bagasse and Synthesized Hydroxyapatite

The FTIR spectrum of the sugarcane bagasse activated carbon (ASB) produced by phosphoric acid activation is shown in Figure 1. O-H stretching vibrations may be responsible for the wide absorption band between 3200 and 3500 cm^{-1}. Aliphatic C-H stretching was responsible for the peaks at 2853 cm^{-1} and 2939 cm^{-1}. The C=C stretching vibration in ASB may be responsible for the absorption band at 1625 cm^{-1}. The bands at 567 cm^{-1}, 602 cm^{-1}, and 865 cm^{-1} are caused by the aromatic rings' C-H plane deformation mode (Yakout and El-Deen, 2016). The peak at 1042 cm^{-1} might be attributed to the symmetrical vibration in the polyphosphate chain of P- O-P and to P^{+}-O^{-} in acid phosphate esters (Puziy *et al.*, 2006).

Figure 2 shows the synthetic hydroxyapatite's FT-IR spectrum. Three key functional groups of phosphate group (PO_4^{3-}), hydroxyl group (OH^-),

and carbonate group (CO_3^{2-}) are frequently used to describe the FT-IR spectra of synthetic hydroxyapatite (Fathi and Hanifi, 2007).

The corresponding peaks observed at 561, 608, 868 and 957 cm^{-1} are associated with P-O bond (Mehta and George, 2013). The peaks found in the region of 3400-3600 cm^{-1} was attributed to O-H stretching bond. The presence of NH_4^+ may be seen in the band at 1600 cm^{-1} (Pramanik *et al*., 2005). The carbonate group is present in the synthesized HAP, as shown by the absorption band found in the 1413–1467 cm^{-1} region. The phosphate group is verified by the recognizable absorption band at 1033 cm^{-1}.

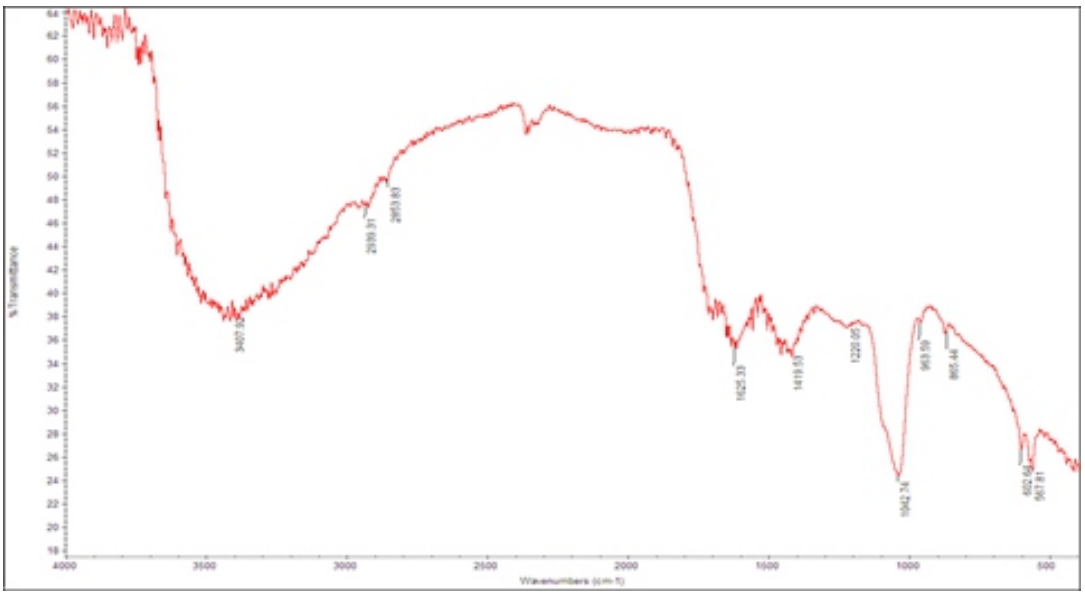

Figure 1: Fourier transform infrared spectrum of ASB.

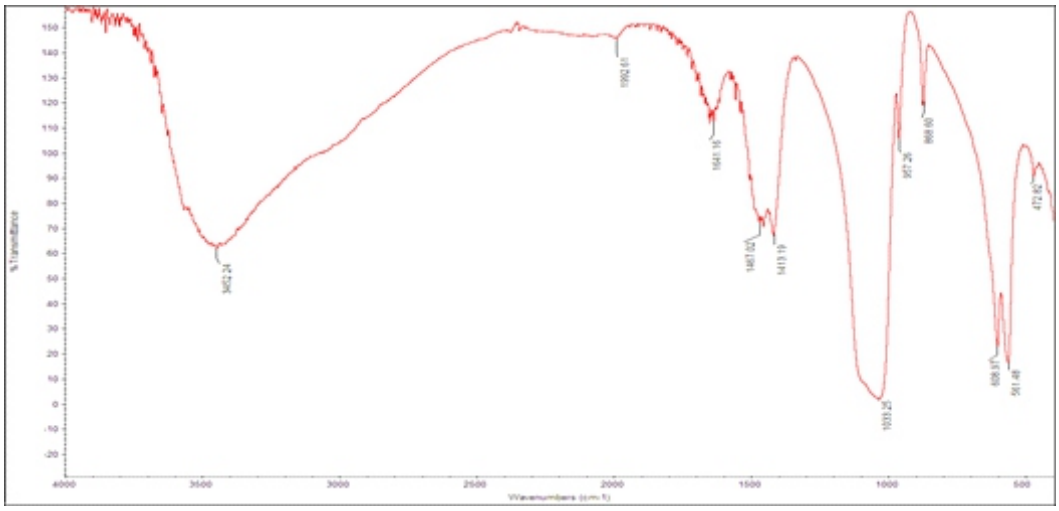

Figure 2: Fourier transform infrared spectrum of HAP.

Scanning Electron Microscopy

The morphological analysis of HAP particle was conducted using scanning electron microscopy (SEM). The hydroxyapatite particles produced were substantially agglomerated, as seen in Figure 3. The Ostwald ripening process may be the cause of the nanoparticle aggregation. The SEM investigation reveals the sphere-shaped particles with clumped distributions. The SEM images demonstrated the spherical-shaped particles that Farraz *et al.* (2004) had previously shown in their SEM micrograph of hydroxyapatite.

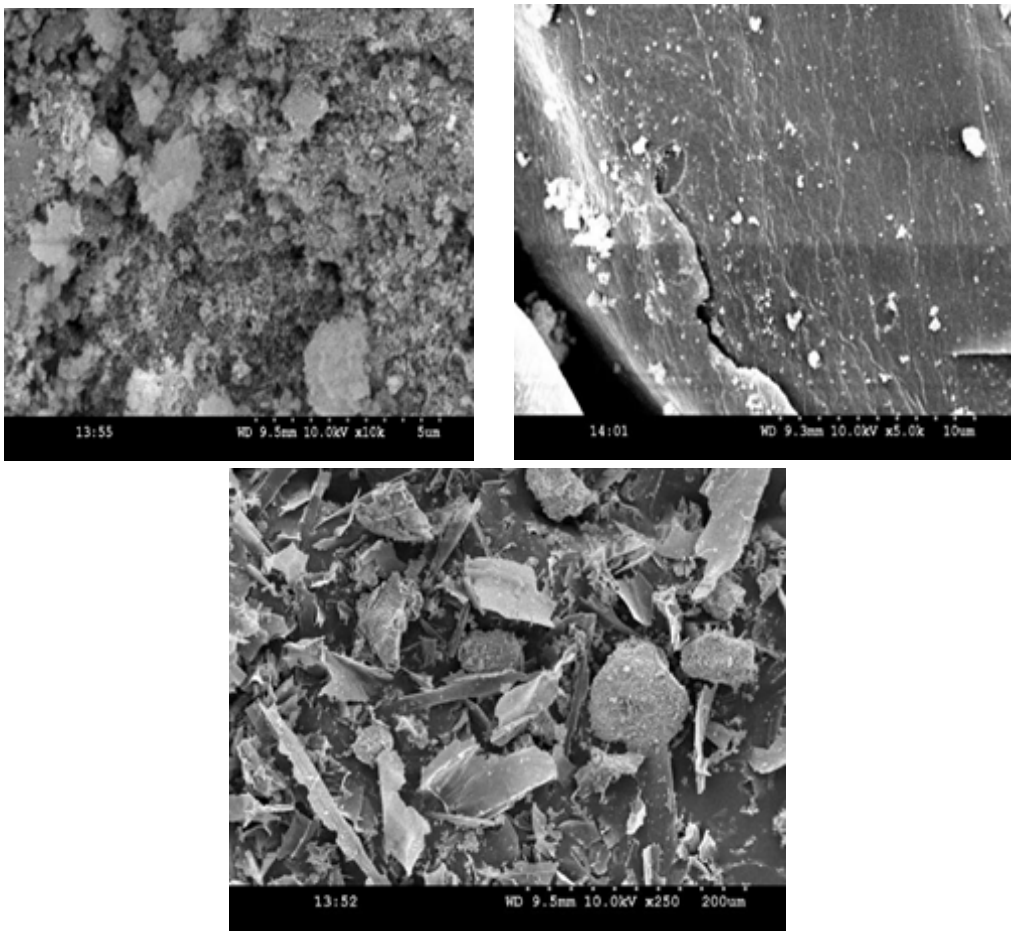

Figure 3: SEM micrograph of HAP at different magnifications at 5 μm to 200 μm.

The SEM micrographs of ASB are presented in Figure 4, it showed that the activated carbon has uneven and porous surface. The activated carbon has number of pores, defects and vacancies; this is expected to contain highly active site to support the adsorption properties. The SEM micrograph of ASB conforms with the morphology that was reported by Thuan *et al.* (2016).

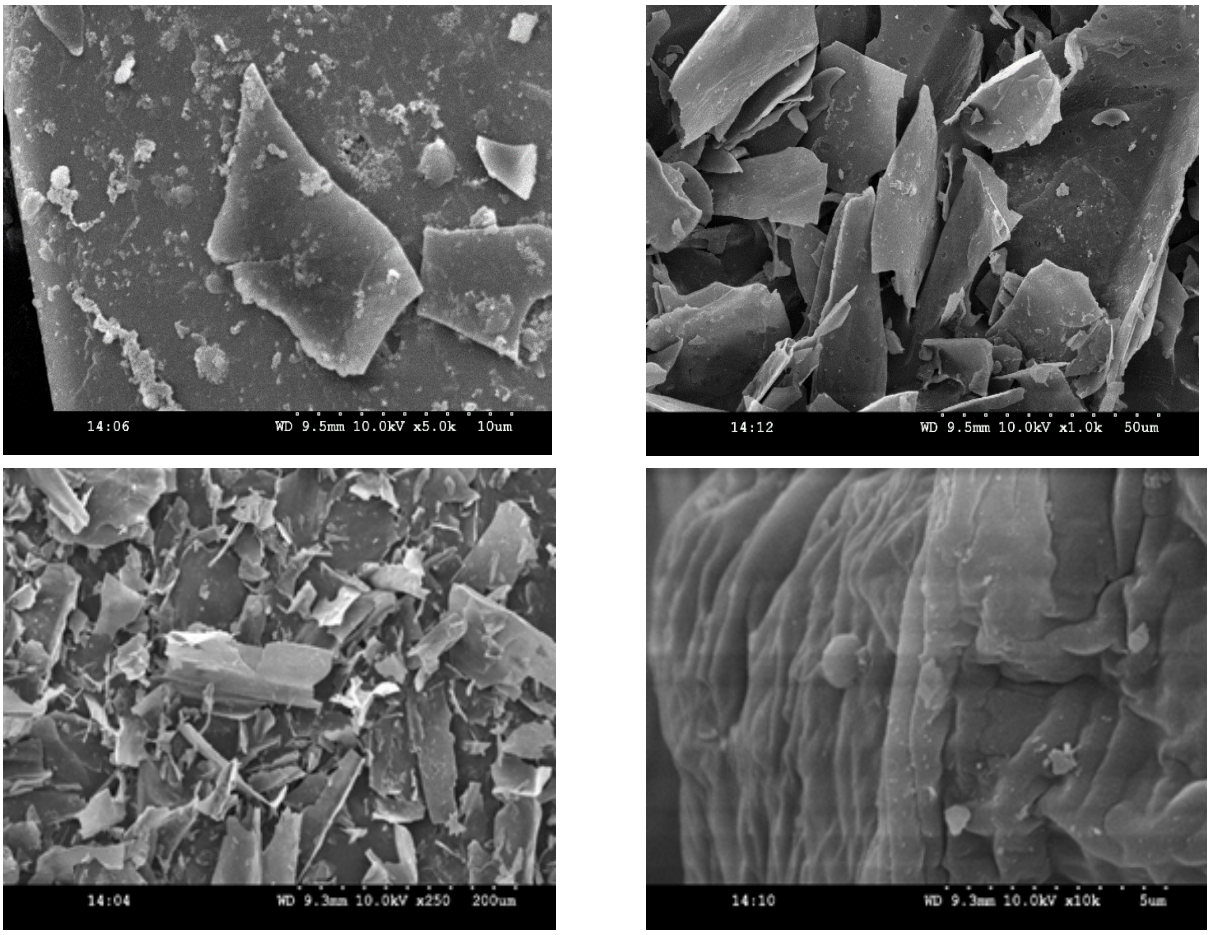

Figure 4: SEM micrograph of ASB at different magnifications at 5 μm to 200 μm.

X-Ray Diffraction (XRD) results

According to JCPDS data No. 09-432, the synthetic adsorbent's X-ray pattern matches the distinctive peaks of pure HAP. A clear peak at 2θ = 26° verifies the synthesis of a single phase stoichiometric HAP with a Ca/P molar ratio of 1.67. These peaks are extremely crystalline with hexagonal phase (Salimi *et al.*, 2012).

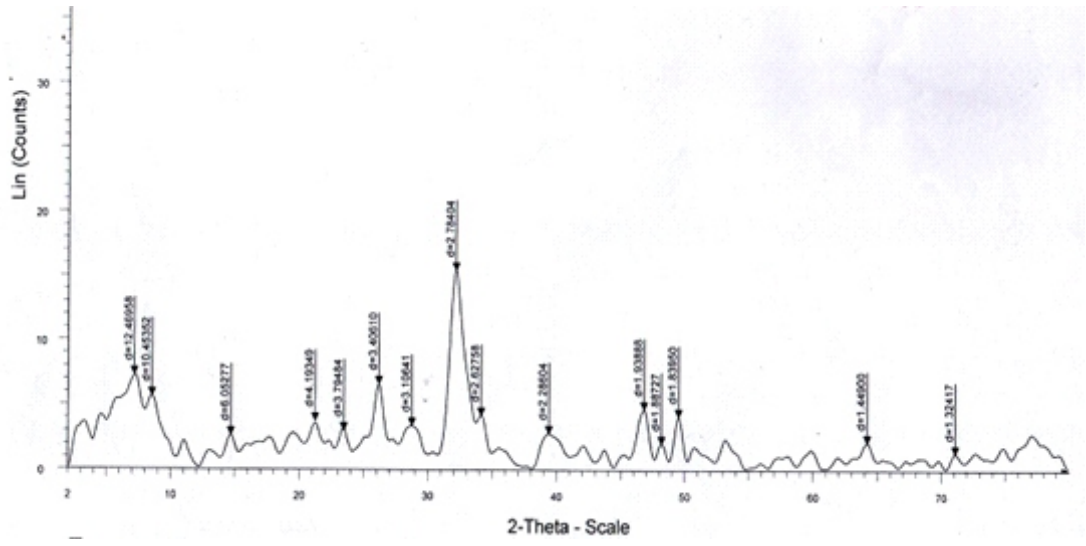

Figure 5: XRD pattern of HAP.

Adsorption of Cr (VI) and Fe (III) on HAP, ASB and their composites

Influence of initial concentration

By varying the metal ion concentration between 5–100 mg/L while maintaining the other experimental conditions constant, the effect of initial concentration on the adsorption of Cr (VI) and Fe (III) was examined [Figures 6(a) and (b)]. The increase in initial concentration led to an increase in the adsorption of Cr (VI) and Fe (III) onto HAP, ASB and ncpA.

This is explained by an increase in the adsorption process's driving force, which rises as the gradient of metal ion concentration does (Liu *et al*., 2019). Nevertheless, the equilibrium adsorption capacity of the three adsorbents for the removal of Cr (VI) was attained at 20 mg/L with an adsorption capacity of 28.26 mg/g, 20.55 mg/g, and 11.83 mg/g for ASB, HAP, and ncpA, respectively. The equilibrium adsorption capacity for the elimination of Fe (III) was discovered at 100 mg/L, with adsorption capacities of 91.57 mg/g, 87.27 mg/g, and 71.80 mg/g for ASB, HAP and ncpA, respectively.

Thus, it can be deduced from the plots that the adsorption capacities of the three adsorbents are in the order: ASB>HAP>ncpA. This indicates that activated carbon of sugarcane adsorbed more than the hydroxyapatite and its composites. The effectiveness of ASB can be as a result of its larger surface area (Table 1) as compared with other adsorbents. Further adsorption investigations employed the equilibrium concentration of 20 mg/L and 100 mg/L.

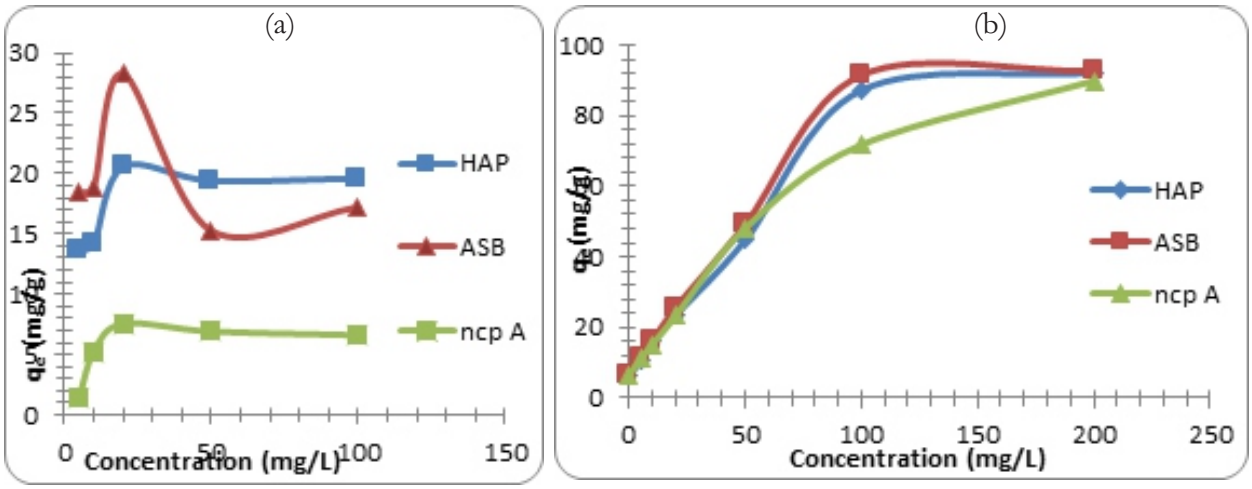

Figure 6: Effect of initial concentration on adsorption of Cr (VI) (a) and Fe (III) (b) onto HAP, ASB and ncpA.

Effect of Adsorbent dosage

As the adsorbent dose was raised, the quantity of Cr (VI) and Fe (III) adsorbed per unit mass of the adsorbents fell dramatically for HAP, ASB, and ncpA [Figures 7(a) and (b)], while the initial concentration of metal ions remained constant. Adsorption site aggregation or overlap may be the cause of the reduction in adsorption capacity with an increase in adsorbent dose (Das and Mondal, 2011).

For the adsorbent HAP, a reduction in its adsorption capacity was observed from 28.91 – 2.36 mg/g for Cr (VI) and from 145.93 – 9.25 mg/g for Fe (III). The experimental results presented in Figures 7(a) and (b) also show a reduction in adsorption capacity of ASB from 25.51 – 2.91 mg/g for Cr (VI) and from 139.65 – 8.33 mg/g for Fe (III) with respect to increase in adsorbent dosage. Similarly, for ncpA, it decreases from 10.02 – 1.14 mg/g for Cr (VI) and from 141.05 – 9.23 mg/g for Fe (III). It is obvious from the results that the extent of uptake of Fe (III) by the three adsorbents was significantly higher than Cr (VI). For the removal of Cr (VI) and Fe (III), the optimal adsorbent dosage was 10 mg; at higher doses, there were fewer metal ions available to

interact with the active sites of the adsorbents, which reduced the adsorption process (Dim *et al.*, 2021). A similar observation was reported from other studies (Ulatowska *et al.*, 2021).

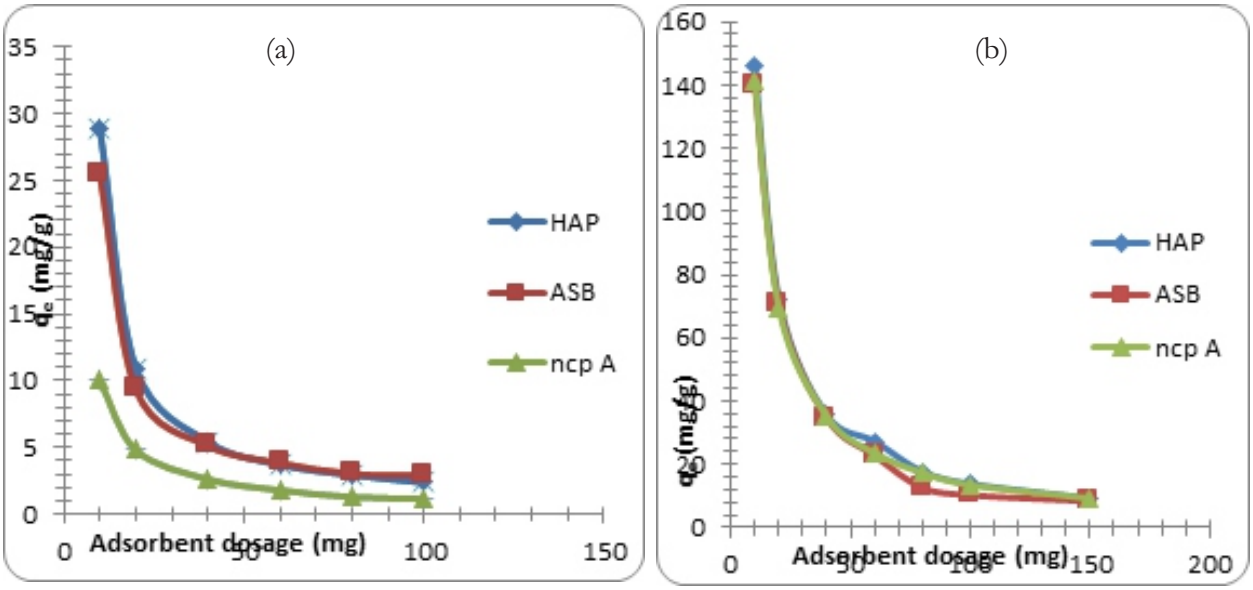

Figure 7: Effect of adsorbent dosage on adsorption of Cr (VI) (a) and Fe (III) (b) onto HAP, ASB and ncpA.

Effect of pH on Adsorption of Cr (VI) ion

The pH of the solution was varied from 1 to 8 to examine the impact of pH on the removal of Cr (VI) and Fe (III). Other experimental variables, such as the initial metal ions concentration of 20 mg/L for Cr (VI) and 100 mg/L for Fe (III), the adsorbent dose of 10 mg, the contact period of 120 min, and the agitation speed of 150 rpm were all held constant throughout these experiments.

It is evident from Figure 8(a) that when the pH of the adsorbate solution increased, the adsorption capacity of the adsorbents dropped. With maximum adsorption capacities of 19.12 mg/g, 16.99 mg/g, and 12.49 mg/g, respectively, the maximum removal of Cr (VI) onto HAP, ASB, and ncpA was discovered at pH 2 to 3.

This could be attributed to the adsorbents' surface charge and the speciation of chromium in aqueous solution. The dominant form of Cr (VI) in a strongly acidic medium (pH 3 to 6) is $HCrO_4^-$ (Rakhunde *et al.*, 2012). The effective metal ion adsorption behavior of the adsorbents in the acidic solution was caused by a significant electrostatic interaction between the positively charged adsorbent surface and $HCrO_4^-$. The results of other studies corroborate this (Adegoke *et al.*, 2014; Ulatowska *et al.*, 2021).

The pH_{pzc} of HAP and ASB was found to be 7.9 and 6.8, respectively. This shows that the surfaces of the adsorbents were positively charged at pH values lower than pH_{pzc}, which facilitated the adsorption of Cr (VI) in an acidic medium. Conversely, at pH greater than pH_{pzc}, the adsorbents' surfaces exhibited a net negative charge, which caused an electrostatic repulsion between them and Cr (VI) with negative charge at alkaline medium. This explains why metal ion adsorption in the alkaline medium is low.

As presented in Figure 8(b), the removal of Fe (III) by the three adsorbents followed different pattern. The adsorption capacities of HAP, ASB and ncpA rose with increase in pH of the reaction solution until pH 4, beyond which the adsorption of metal ions was as result of the precipitation of the complex of iron as $Fe(OH)_3$. Consequently, the precipitated metal hydroxide complex could appear as evidently greater metal ion adsorption (Hizal and Apak, 2006; Srivastava, 2008).

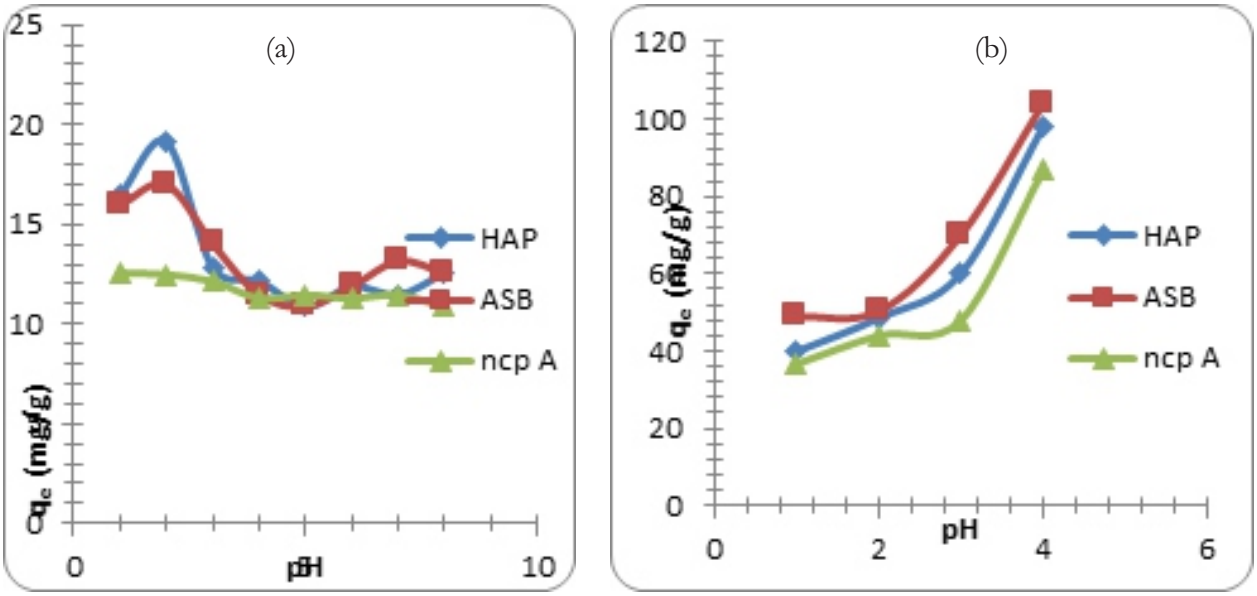

Figure 8: Effect of pH on Removal of Cr (VI) (a) and Fe (III) (b) onto HAP, ASB and ncpA.

Effect of Contact Time

In a batch adsorption experiment, it is crucial to ascertain the contact time required to reach equilibrium. Figures 9(a) and (b) show the findings of a study on the impact of contact time on the adsorption of Cr (VI) and Fe (III) throughout a time range of 30–240 min. The adsorption of metal ions increases with the contact time with optimal adsorption achieved at 60 min for Fe (III) removal on HAP, ASB and ncpA. The results of Wang *et al.* (2017) lend credence to this, that the optimal adsorption time required for the uptake of Fe (III) from aqueous medium was 60 min. Similarly, for Cr (VI) uptake, optimum adsorption was reached at 60 min for the adsorbents except for ncpA which was observed at 120 min; further lengthening of the contact time had no appreciable impact or even decreased the adsorption capacity. The strong solute concentration gradient and empty pore gaps were the causes of the quick adsorption process (Dim *et al.*, 2021). The saturation of the functional groups and activated sites present on the surface of the adsorbents later resulted in slow uptake of metal ions.

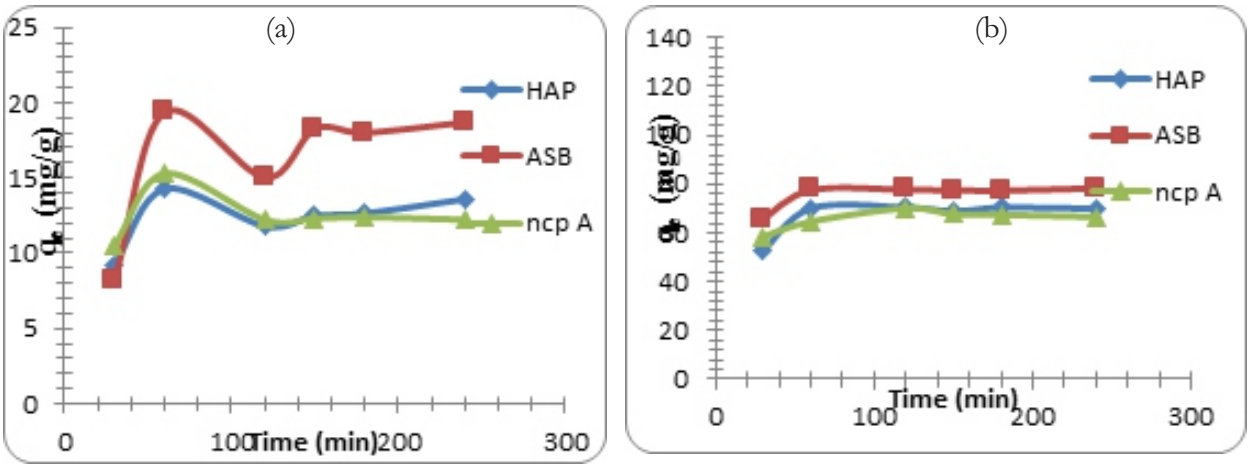

Figure 9: Effect of contact time on adsorption of Cr (VI) (a) and Fe (III) (b) onto HAP, ASB and ncpA.

Effect of Temperature

Presented in Figures 10(a) and (b), are the plots of the influence of temperature on the removal of Cr (VI) and Fe (III) onto HAP, ASB and ncpA at optimum experimental conditions. The correlation of the adsorption potential of the adsorbents as a function the temperature was studied between 293–340 K. The adsorption capabilities of HAP, ASB, and ncpA were found to increase when the solution temperature rose from 293 to 340 K, as seen in the Figures, indicating that higher temperatures are favorable for the adsorption of Cr (VI) and Fe (III) on the adsorbents. These observations suggested that the adsorption of Cr (VI) and Fe (III) ions was an endothermal adsorption process with a chemisorption mechanism. Gupta *et al.* (2012) and Igwebe *et al.* (2013) also noted the same pattern. As a result, raising the temperature of adsorption reduces the viscosity of the solution, enabling the diffusion of adsorbate molecules through the adsorbent's exterior boundary layer and enhancing the adsorption of metal ions (Rashed *et al.*, 2019). Moreover, raising the temperature may cause the mesoporous structure of the adsorbents to enlarge, which would increase the adsorption of metal ions.

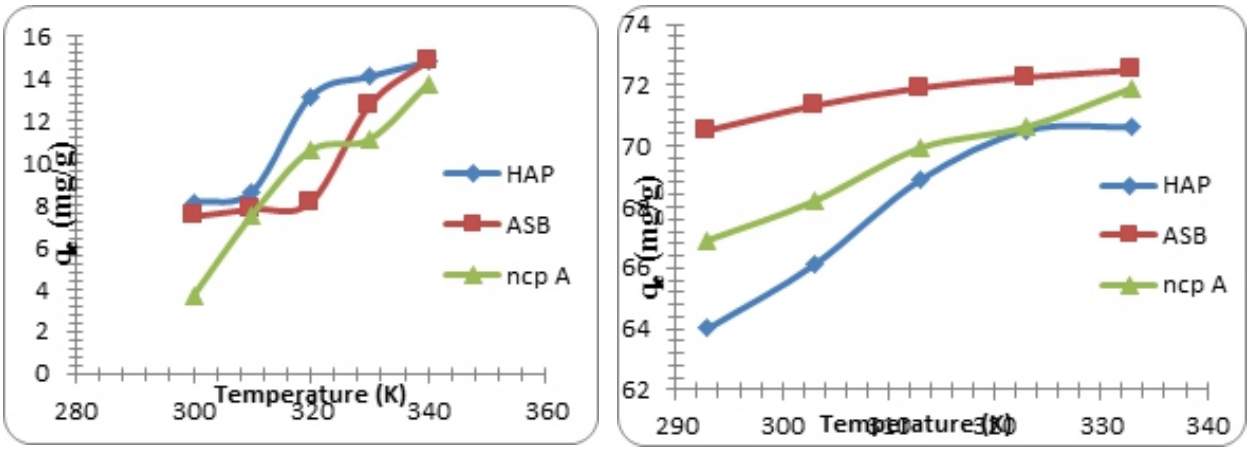

Figure 10: Effect of Temperature on Adsorption of Cr (VI) (a) and Fe (III) (b) onto HAP, ASB and ncpA.

Adsorption Isotherm

The equilibrium data from the adsorption of Cr (VI) and Fe (III) onto HAP, ASB, and ncpA were modeled into the Langmuir (Eq. 2) and Freundlich models (Eq. 4), in order to comprehend the process involved in the adsorption of the metal ions.

$$\frac{C_e}{q_e} = \frac{1}{K_L q_m} + \frac{1}{q_m} C_e \qquad (2)$$

Where K_L (Lmg^{-1}) is the Langmuir constant, which measures the affinity for the binding sites (Abuzalat *et al.*, 2022), q_e (mgg^{-1}) is the quantity of metal ions adsorbed per unit mass of the adsorbents, q_m (mgg^{-1}) is the maximum monolayer adsorption capacity. The slope and intercept of the plot of C_e/q_e against Ce (equilbrium concentration) are used to determine the values of q_m and K_L.

An important component of the Langmuir isotherm is the separation factor R_L, which is calculated by Eq (3).

$$R_L = \frac{1}{1 + K_L C_0} \qquad (3)$$

$$\text{Log } q_e = Log\ K_f + (\frac{1}{n}) \text{ Log } C_e \qquad (4)$$

In a heterogeneous system, adsorption process is described by the Freundlich isotherm model (Ali *et al.*, 2021). 1/n is the heterogeneity parameter, If value of $1/n < 1$, it indicates a normal adsorption, and if $1/n > 1$ it indicates cooperative adsorption (Adebayo *et al.*, 2020). K_f is the Freundlich constant, it determines the adsorption capacity of the adsorbents.

The evaluated parameters are summarized in Table 2. According to the correlation coefficient values (R^2), the equilibrium data for Cr (VI) removal onto the adsorbents fitted best into the Langmuir isotherm model, revealing good

monolayer coverage. The maximum monolayer adsorption capacities of HAP, ASB and ncpA for Cr (VI) removal was 19.92 mg/g, 16.69 and 10.33 mg/g respectively. The favorability of an adsorption process is determined by the separation factor (R_L). If $R_L > 1$, the adsorption is unfavorable; if $R_L = 1$, it is linear; if $R_L < 1$, it is favorable; and if $R_L < 0$, it is irreversible (Dada *et al*., 2017). The R_L values found in this investigation were smaller than unity, indicating that metal ions were successfully adsorbed.

However, the equilibrium data for the uptake of Fe (III) on the adsorbents also fitted to the Langmuir isotherm model but not as the Freundlich isotherm model. Based on the correlation coefficient values (R^2) in Table 2, the equilibrium data for ncpA fitted best into the model with 0.9764, followed by that of HAP with 0.9681,and ASB with 0.9381 for Fe (III) removal, suggesting an heterogeneous adsorption (Kong *et al*., 2017). The Freundlich constant (K_F) was 5.14 mg/g, 9.24 mg/g and 5.27 mg/g and heterogeneity parameter (1/n) was 0.55, 0.52 and 0.54 for the uptake of Fe (III) onto HAP, ASB and ncpA mg/g respectively. The values of 1/n which was below unity indicate a normal adsorption process. The values of the adsorption intensities (n) in the range of 1 to 10 obtained in this study, confirms that the removal of Cr (VI) and Fe (III) was conducted under favourable experimental conditions.

Table 2: Adsorption isotherm parameters for the uptake of Cr (VI) and Fe (III) onto HAP, ASB, and ncpA

Model	Parameter	Cr(VI)			Fe(III)		
		HAP	ASB	ncpA	HAP	ASB	ncpA
Langmuir	q_{max} (mg/g)	19.92	16.69	10.33	113.64	113.64	107.53
	K_L (Lmg^{-1})	0.145	0.136	0.777	0.023	0.021	0.021
	R_L	0.147	0.161	0.031	0.308	0.328	0.319
	R^2	0.9981	0.9880	0.9515	0.8945	0.8764	0.9047
Freundlich	K_f (Lmg^{-1})	8.66	6.62	0.47	5.14	9.24	5.27
	1/n	0.189	0.291	0.649	0.554	0.5212	0.5374
	n	5.29	3.44	1.54	1.8051	1.9381	0.9764
	R^2	0.8139	0.5110	0.7120	0.9681	0.9381	0.9764

Adsorption Kinetics

The experimental data at different contact times were fitted into pseudo-first order (5) and pseudo-second order (6) models to ascertain the mechanism and the rate-controlling step in the adsorption of Cr (VI) and Fe (III) onto HAP, ASB, and ncpA.

$$\ln (q_e - q_t) = \ln q_e - k_1 t \quad (5)$$

$$\frac{t}{q_t} = \frac{1}{k_2 q_e^2} + \frac{1}{q_e} t \quad (6)$$

Where k_1 (min^{-1}) is the pseudo-first-order rate constant and k_2 (g/mgmin) is the rate constant of the pseudo-second-order kinetic model; q_e and q_t are the quantities of metal ions adsorbed (mg/g) at equilibrium and time t, respectively as shown in Table 3 for the metal ions adsorbed.

Statistical Rationality of Kinetic Models Data

Scrutinizing the best fittings and agreement between kinetic data, the non-linear chi square test (χ^2) and statistical tools like correlation coefficients (R^2), sum of square errors (SSE) were

utilized (Dada *et al.*, 2020). These statistical models are expressed with equations 7 and 8.

$$SSE = \sum_{i=1}^{n} (q_{e\,cal} - q_{e\,exp})^2 \quad (7)$$

$$\chi^2 = \sum_{i=1}^{n} \frac{(q_{e\,exp} - q_{e\,cal})^2}{q_{e\,cal}} \quad (8)$$

Where, $q_{e\,cal}$ is the amount of metal ions adsorbed calculated from the kinetic models equations and $q_{e\ exp}$ is the experimental quantity of metal ions adsorbed at equilibrium.

The fitness of the two models was tested by a plot of ln (q_e - q_t) against t (Pseudo-first-order model) and t/q_t against t (Pseudo-second-order model). The parameters of the kinetic model were determined and are shown in Table 3. For the pseudo-second-order kinetic model, the correlation coefficients (R^2) values were nearly equal to one, for Cr (VI), it was 0.9906, 0.9652 and 0.9964 while that of Fe (III) was 0.9982, 0.9995 and 0.9987 for their adsorption onto HAP, ASB and ncpA respectively. These findings demonstrated that the pseudo-second-order kinetic model more accurately predicted the adsorption of Cr (VI) and Fe (III) onto the adsorbents, indicating that chemisorption was the rate-limiting phase. The good agreement between experimental and the calculated q_e values also indicated the suitability of pseudo-second-order model. The validity of pseudo-second-order model is supported by the small values of SSE and χ^2 for all the adsorption systems (Dada *et al.*, 2020).

Table 3: Kinetic parameters for the different adsorbents on Cr (VI) and Fe (III).

Model	Parameter	Cr (VI)			Fe (III)		
		HAP	ASB	nCPA	HAP	ASB	nCPA
	q_e exp (mg/g)	14.27	19.38	15.29	70.52	77.73	70.17
Pseudo-first order	q_e calc. (mg/g)	12.66	18.27	12.40	0.98	0.99	0.99
	K_1 (min^{-1})	-1.937	-2.308	-1.707	-2.425	-2.378	-2.599
	R^2	0.6063	0.4543	0.1634	0.5525	0.5576	0.9816
	SSE	2.592	1.232	8.179	4835.81	5889.03	4785.87
	X^2	0.204	0.067	0.67	4934.50	5948.51	4834.22
Pseudo-first order	q_e calc. (mg/g)	13.42	19.65	12.23	71.43	78.79	67.57
	K_2(g/mg.min^{-1})	0.0115	0.0029	0.0525	0.0040	0.0056	0.0133
	R^2	0.9906	0.9652	0.9964	0.9982	0.9995	0.9987
	SSE	0.723	0.073	9.364	0.8281	1.124	6.76
	X^2	0.054	0.0037	0.766	0.012	0.014	0.100

Table 4: Comparison of various adsorbents for removal of Cr (VI) and Fe (III).

Adsorbent	Metal ions	q_e (mgg^{-1})	Rate Constant (g/mgmin)	References
HAP	Cr (VI)	19.92	0.0115	Current Study
ASB	Cr (VI)	16.69	0.0029	Current Study
ncpA	Cr (VI)	10.33	0.0525	Current Study
Schwertmannite	Cr (VI)	17.54	0.0007	Ulatowska *et al*.,2021
Olive Stone-Sulfuric acid AC	Cr (VI)	71.4	0.008	Attia *et al*., 2010
Nano hydroxyapatite	Cr (VI)	1.24	0.007	Asgari *et al*., 2012
Coconut shell AC	Cr (VI)	4.75	2.6×10^{-4}	Tang *et al*., 2009
Hydrochloric acid modified clay	Cr (VI)	18.15	1.679	Dim *et al*., 2021
Rice husk	Cr (VI)	12.63	-	Shrivastava and Gupta (2015)
HAP	Fe (III)	113.64	0.0040	Current Study
ASB	Fe (III)	113.64	0.0056	Current Study
ncpA	Fe (III)	107.53	0.0133	Current Study
Hydrochloric acid modified clay	Fe (III)	39.8	0.526	Dim *et al*., 2021
Xanthoceras Sorbifolia Bunge AC	Fe (III)	241.13	1.1295 × 10-4	Tang *et al.,* 2017
Thiourea cross-linked Chitosan	Fe (III)	71.9	0.0019	Dai *et al*., 2012
Zeolite	Fe (III)	10.19	-	Bakalar *et al*., 2020
Bentonite	Fe (III)	11.64	-	Bakalar *et al*., 2020
Polyaniline coated sawdust	Fe (III)	40.65	-	Mansoor and Abbasitabar (2020)

CONCLUSION

The study has successfully prepared and characterized hydroxyapatite (HAP), activated carbon (ASB) and their composite (ncpA) for wastewater treatment applications. The FT-IR analysis showed that the adsorbents had a variety of functional groups that can facilitate the adsorption of Cr (VI) and Fe (III) from aqueous solution. The remarkable crystallinity of the synthetic hydroxyapatite was revealed by the XRD analysis. Investigations were conducted to determine how the initial concentration of metal ions, adsorbent dose, pH, contact time, and temperature affected the adsorption process. The adsorbate uptake increased with increase in initial metal ions concentration and the contact time. Both the Langmuir and Freundlich isotherm models provided accurate descriptions of the adsorption process. Based on the Langmuir separation factor, R_L, the adsorption process was a favorable process. The kinetic data was best fitted into the pseudo-second-order as validated by sum of square error (SSE) and non-linear chi-square (χ^2). The research demonstrated the efficacy of HAP, ASB, and ncpA as an environmentally friendly, economically viable, and sustainable adsorbent for wastewater remediation.

REFERENCES

Abuzalat, O. Wong,D., Elsayed, A.M., 2022. Nano-Porous Composites of Activated Carbon–Metal Organic Frameworks (Fe-BDC@AC) for Rapid Removal of Cr (VI): Synthesis, Adsorption, Mechanism, and Kinetics Studies. *Journal of Inorganic and Organometallic Polymers and Materials*. 32, 1924–1934.
doi: 10.1007/s10904-022-02237-9

Adebayo, G. B., Adegoke, H. I., Jamiu, W., Balogun, B. B., Jimoh, A. A., 2015. Adsorption of Mn (II) and Co (II) ions from aqueous solution using maize cob activated carbon: kinetics and thermodynamics studies. *Journal of Applied Sciences and Environmental Management*. 19(4), 737–748.
doi: 10.4314/jasem.v19i4.22

Adebayo, G. B., Adegoke, H. I., Fauzeeyat, S., 2020. Adsorption of Cr (VI) ions onto goethite, activated carbon and their composite: kinetic and thermodynamic studies. Applied Water Science, 10(9), 1–18.
doi: 10.1007/s13201-020-01295-z

Adegoke, H. I., Adekola, F. A., Fatoki, O. S., Ximba, B. J., 2014. Adsorption of Cr (VI) on synthetic hematite (α-Fe_2O_3) nanoparticles of different morphologies. *Korean Journal of Chemical Engineering*. 31(1),142–154. doi: 10.1007/s11814-013-02047

Agrawal, K., Singh, G., Puri, D., Prakash, S., 2011. Synthesis and Characterization of Hydroxyapatite Powder by Sol-Gel Method for Biomedical Application. *Journal of Minerals & Materials Characterization & Engineering*. 10,727–734. doi: 10.4236/jmmce.2011.108057

Aldawsari, A. M., Alsohaimi, I. H., Al-Kahtani, A. A., Alqadami, A. A., Ali Abdalla, Z. E., & Saleh, E. A. M. (2021). Adsorptive performance of aminoterephthalic acid modified oxidized activated carbon for malachite green dye: mechanism, kinetic and thermodynamic studies. *Separation Science and Technology*, *56*(5), 835–846. doi: 10.1080/01496395.2020.1737121

Ali, H. M., Essawy, A. A., Elnasr, T. A. S., Aldawsari, A. M., Alsohaimi, I., Hassan, H. M., Abdel-Farid, I. B.,2021. Selective and efficient sequestration of Cr (VI) in ground water using trimethyloctadecylammonium bromide impregnated on Artemisia monosperma plant powder. *Journal of the Taiwan Institute of Chemical Engineers*, 125, 122–131. doi: 10.1016/j.jtice.2021.05.051

Alothman, Z.A., Bahkali, A.H., Khiyami, M.A., Alfadul, S.M., Wabaidur, S.M., Alam, M., Alfarhan, B.Z.,2020. Low cost biosorbents from fungi for heavy metals removal from wastewater, *Sep. Sci. Technol.* 55, 1766–1775 . doi:10.1080/01496395.2019.1608242

Asgari, G., Rahmani, A. R., Faradmal, J., Seid, M. A., 2012. Kinetic and isotherm of hexavalent chromium adsorption onto nano hydroxyapatite, *Journal of Research Health Sciences*, 45–53.

Attia, A. A., Khedr, S. A., Elkholy, S. A., 2010. Adsorption of chromium ion (VI) by acid activated carbon. *Brazilian Journal of Chemical Engineering*. 27, 183–193. doi: 10.1590/S0104-66322010000100016

Aziz, A., Ouali, M. S., Elandaloussi, E. H., De Menorval, L. C., Lindheimer, M., 2009. Chemically modified olive stone: A low-cost sorbent for heavy metals and basic dyes removal from aqueous solutions. *Journal of hazardous materials*, 163(1), 441–447. doi: 10.1016/j.jhazmat.2008.06.117

Bakalár, T., Kaňuchová, M., Girová, A., Pavolová, H., Hromada, R., Hajduová, Z.,2020. Characterization of Fe (III) adsorption onto zeolite and bentonite. *International Journal of Environmental Research and Public Health*. 17(16), 5718. doi: 10.3390/ijerph17165718

Baseri, J. R., Palanisamy, P. N., Sivakumar, P., 2012. Preparation and characterization of activated carbon from Thevetia peruviana for the removal of dyes from textile waste water. *Advances in Applied Science Research*, 3(1), 377–383.

Bello, M. O., Abdus-Salam, N., Adekola, F. A.,Pal,U., 2021. Isotherm and kinetic studies of adsorption of methylene blue using activated carbon from ackee apple pods. *Chemical Data Collections*, 31, 100607. doi:10.1016/j.cdc.2020.100607

Bello, O. S., Alabi, E. O., Adegoke, K. A., Adegboyega, S. A., Inyinbor, A. A., Dada, A. O. 2020. Rhodamine B dye sequestration using Gmelina aborea leaf powder. *Heliyon*, 6(1), 02872. doi: 10.1016/j.heliyon.2019.e02872

Chen, C.-X., Huang, B., Li, T., and Wu. G.-F. 2012. Preparation of phosphoric acid activated carbon from sugarcane bagasse by mechanochemical processing. *BioRes.* 7(4), 5109–5116.

Dada, A. O., Adekola, F. A., Odebunmi, E. O., Dada, F. E., Bello, O. M., Akinyemi, B. A., Umukoro, O. G.,2020. Sustainable and low-cost Ocimum gratissimum for biosorption of indigo carmine dye: kinetics, isotherm, and thermodynamic studies. *International Journal of Phytoremediation*. 22(14), 1524–1537. doi.:10.1080/15226514.2020.1785389

Dada, A.O., Adekola, F. A., Odebunmi, E.O., 2017. Liquid Phase Scavenging of Cd (II) and Cu (II) ions onto novel nanoscale zerovalent manganese (nZVMn): Equilibrium, Kinetic and Thermodynamic Studies. *Environmental Nanotechnolgy, Monitoring and Management* 8, 63–82. doi:10.1016/j.enmm.2017.05.001

Dai, J., Ren, F., Tao, C., 2012. Adsorption behavior of Fe (II) and Fe (III) ions on thiourea cross-linked chitosan with Fe (III) as template. *Molecules*, 17(4), 4388–4399. doi: 10.3390/molecules17044388

Das, B., Mondal, N. K., 2011. Calcareous Soil as a New Adsorbent to Remove Lead from Aqueous Solution: Equilibrium, Kinetic and Thermodynamic Study. *Universal Journal of Environmental Research & Technology*. 1 (4), 515–530.

Dim, P. E., Mustapha, L. S., Termtanun, M., & Okafor, J. O., (2021). Adsorption of chromium (VI) and iron (III) ions onto acid-modified kaolinite: Isotherm, kinetics and thermodynamics studies. *Arabian Journal of Chemistry*, 14(4), 103064. doi:10.1016/J.ARABJC.20t21.103064

Ekpete, O. A., Horsfall, M. J. N. R., 2011. Preparation and characterization of activated carbon derived from fluted pumpkin stem waste (Telfairia occidentalis Hook F). *Res J Chem Sci.* 1(3), 10–17. www.isca.in

Eletta, O. A., Ayandele, F. O., Ighalo, J. O., 2021. Adsorption of Pb (II) and Fe (II) by mesoporous composite activated carbon from Tithonia diversifolia stalk and Theobroma cacao pod. Biomass Conversion and Biorefinery, 1–10. doi:10.1007/s13399-021-01699-0

Farahani, M., Abdullah S.R., Hosseini S., Kashisaz, M. 2011.Adsorption-based Cationic Dyes using the Carbon Active Sugarcane Bagasse. 2011. *Procedia Environmental Sciences* 10:203–208 doi:10.1016/j.proenv.2011.09.035

Fathi, M. H., Hanifi, A. (2007). Evaluation and characterization of nanostructure hydroxyapatitepowder prepared by simple sol–gel method. Materials letters, 61(18), 3978–3983. doi:10.1016/j.matlet.2007.01.028

Ferraz, M. P., Monteiro, F. J., Manuel, C. M., 2004. Hydroxyapatite nanoparticles: a review of preparation methodologies. *Journal of Applied Biomaterials and Biomechanics*, 2(2), 74–80.

Gupta, N., Kushwaha, A. K., Chattopadhyaya, M. C., 2012. Adsorptive removal of Pb^{2+}, Co^{2+} and Ni^{2+} by hydroxyapatite/chitosan composite from aqueous solution. *Journal of the Taiwan Institute of Chemical Engineers*, 43(1), 125–131. doi:10.1016/J.JTICE.2011.07.009

Gusain, D.; Verma, V.; Uma; Bux, F.; Sharma, Y.C., 2020. A novel approach for the removal of chromium (VI) from aqueous solutions using nano iron oxide. *Int. J. Environ. Anal. Chem.* 1–16. doi:10.1080/03067319.2020.1761644

Hizal, J., Apak, R., (2006). Modeling of cadmium (II) adsorption on kaolinite-based clays in the absence and presence of humic acid. *Applied Clay Science*. 32(3-4), 232–244. doi:10.1016/J.CLAY.2006.02.002

Igwegbe, C.A., Ighalo, J.O., Onyechi, K.K.,Onukwuli, O.D., 2021. Adsorption of Congo red and malachite green using H_3PO_4 and NaCl-modified activated carbon from rubber (Hevea brasiliensis) seed shell. *Sustainable Water Resources Management*. 7, 1–16. doi:10.1007/s40899-021-00544-6

Jaishankar, M., Tseten, T.; Anbalagan, N.; Mathew, B.B.; Beeregowda, K.N., 2014. Toxicity, mechanism and health effects of some heavymetals, Interdisciplinary Toxicology. *Interdiscip. Toxicol.* 7, 60–72. doi: 10.2478/intox-2014-0009

Joudi, M., Bensemlali, M., Yassine, I., Hatimi, B., Hafdi, H., Mouldar, J., Bakasse, M., 2022. Adsorption of chromium VI onto hydroxyapatite–chitosan-montmorillonite thin film. Materials Today: Proceedings. doi:10.1016/j.matpr.2022.06.151

Kantar, C., Ari, C., Keskin, S., 2015. Comparison of different chelating agents to enhance reductive Cr (VI) removal by pyrite treatment procedure. Water Res. 76, 66–75.
doi: 10.1016/j.watres.2015.02.058

Khandelwal, H., Prakash, S.,2016. Synthesis and characterization of hydroxyapatite powder by eggshell. *Journal of Minerals and Materials Characterization and Engineering*, 4(2), 119–126.
doi**:** 10.4236/jmmce.2016.42011

Kong, Q., He, X., Shu, L., Sheng, M. M.,2017. Ofloxacin adsorption by activated carbon derived from luffa sponge: kinetic, isotherm, and thermodynamic analyses, Process Saf. *Environ. Prot.*112, 254–264.
doi: 10.1016/J.PSEP.2017.05.011

Kousalya, G. N., Gandhi, M. R., Sundaram, C. S., Meenakshi, S.,2010. Synthesis of nano-hydroxyapatite chitin/chitosan hybrid biocomposites for the removal of Fe (III). Carbohydrate polymers, 82(3), 594–599.
doi:10.1016/j.carbpol.2010.05.013G

Kozlowski, C. A.,Walkowiak, W., 2002. Removal of chromium (VI) from aqueous solutions by polymer inclusion membranes. *Water Research*, 36(19), 4870–4876.
doi:10.1016/S0043-1354(02)00216-6

Labied, R., Benturki, O., Eddine Hamitouche, A. Y., Donnot, A., 2018. Adsorption of hexavalent chromium by activated carbon obtained from a waste lignocellulosic material (Ziziphus jujuba cores): Kinetic, equilibrium,and thermodynamic study. Adsorption science & technology, 36(3-4), 1066–1099.
doi:10.1016/S0043-1354(02)00216-6

Li, Y., Hu, X., Ren, B., Wang, Z., 2016. Removal of high-concentration Fe (III) by oxidized multiwall carbon nanotubes in a fixed bed column. *Am. Chem. Sci. J.* 10, 1–9.

Li, Z., Li, M., Zheng, T., Li, Y., Liu, X., 2019. Removal of tylosin and copper from aqueous solution by biochar stabilized nanohydroxyapatite. Chemosphere. 235,136–142.
doi:10.1016/j.chemosphere.2019.06.091

Liu, Q.X., Zhou, Y.R., Wang, M., Zhang, Q., Ji, T., Chen, T.-Y.,Yu, D.C., 2019. Adsorption of methylene blue from aqueous solution onto viscose-based activated carbon fiber felts: Kinetics and equilibrium studies, *Adsorption Science & Technology*. 37, 312–332.
doi: 10.1177/0263617419827437.

Luana A. R. Giusto, Fábio L. Pissetti,Talita S. Castro and Fabiano Magalhães, 2017 Preparation of Activated Carbon from Sugarcane Bagasse Soot and Methylene Blue Adsorption. *Water, Air, & Soil Pollution* volume 228, Article number: 249

Mane, S. M., Vanjara, A. K., Sawant, M. R., 2005. Removal of phenol from wastewater using date seed carbon. *Journal of the Chinese Chemical Society*, 52(6), 1117–1122.
doi:10.1002/JCCS.200500160

Mansoor, S. J., Abbasitabar, F., 2020. Adsorption Behavior of Fe (II) and Fe (III) Ions on Polyaniline Coated Sawdust: Batch and Fixed–Bed Studies. *Acta Chimica Slovenica*, 67(1), 36–46.
doi: 10.17344/ACSI.2019.5121

Mehta, D., George, S. 2013. Hydroxyapatite: Synthesis and Characterization. International Conference on Materials for the Future - Innovative Materials, Processes, Products and Applications – ICMF 2013

Minas, F., Chandravanshi, B.S., Leta, S. Chemical precipitation method for chromium removal and its recovery from tannery waste water in Ethiopia. Chem. Int. 3, 291–305. ISSN: 2410-9649

Mohamed, K. R., El-Rashidy, Z. M.,Salama, A. A.,2011. In vitro properties of nano-hydroxyapatite/chitosan biocomposites. Ceramics International. 37(8), 3265–3271.
doi:10.1016/j.jare.2013.02.004G

Mortazavian, S., An, H., Chun, D., Moon, J. 2018. Activated carbon impregnated by zero-valent iron nanoparticles (AC/nZVI) optimized for simultaneous adsorption and reduction of aqueous hexavalent chromium: Material characterizations and kinetic studies. *Chemical Engineering Journal*. 353, 781–795.
doi:10.1016/j.cej.2018.07.170

Nageeb, R., Gad, A.A., AbdEldaiem, A.M., 2019. Novel Composite from Glass Waste and Activated Carbon for Heavy Metals Removal from Well Water in Semi-arid Regions. *International Journal of Water Resources and Arid Environments*. 8(1), 39–48.

Narayan, R.J.,Kumta, P.N., Sfeir, C., Lee, D.H., Olton, D., Choi, D.W. 2004. Nanostructured ceramics in medical devices: applications and prospects. JOM. 56,38–43. doi:10.1007/s11837-004-0289

Nasiruddin, K., M., Sarwar, A.,2007. Determination of points of zero charge of natural and treated adsorbents. Surface Review and Letters. 14(03), 461–469. doi:10.1142/S0218625X07009517

Nur-E-Alam, M. Mia, M.A.S. Ahmad, F., Rahman, M.M., 2020. An overview of chromium removal techniques from tannery effluent. Appl. Water Sci., 10, 205. doi:10.1007/s13201-020-01286-0

Prabakaran, K., Balamurugan, A., Rajeswari, S., 2005. Development of calcium phosphate based apatite from hen's eggshell. *Bulletin of Materials Science*, 28(2), 115–119. doi:10.1007/BF02704229

Pramanik, S., Agarwal, A. K., Rai, K. N., 2005. Development of high strength hydroxyapatite for hard tissue replacement. *Trends in Biomaterials and Artificial Organs*. 19(1), 46–51. Corpus ID: 12965878

Puziy, A. M., Poddubnaya, O. I., Martínez-Alonso, A., Castro-Muñiz, A., Suárez-García, F., Tascón, J.M., 2007. Oxygen and phosphorus enriched carbons from lignocellulosic material. Carbon. 45(10), 1941–1950. doi:10.1016/j.carbon.2007.06.014

Raihana, M.F., Sopyan, I., Hamdi, M. and Ramesh, S., 2008. Novel Chemical Conversion of Eggshell to Hydroxyapatite Powder. *International Federation for Medical and Biological Engineering Proceedings*. 21, 333–336. doi:10.1007/978-3-540-691396_85

Rakhunde, R. Deshpande, L. Juneja, H.D., 2012. Chemical speciation of chromium in water: A review. Crit. Rev. Environ. Sci. Technol. 42, 776–810. doi:10.1080/10643389.2010.534029

Ren, Y., Han, Y., Lei, X., Lu, C., Liu, J., Zhang, G., Zhang, Q., 2020.A magnetic ion exchange resin with high efficiency of removing Cr (VI). Colloids and Surfaces A: Physicochemical and Engineering Aspects, 604, 125279.

Sahu, J. N., Acharya, J., Meikap, B. C., 2010. Optimization of production conditions for activated carbons from Tamarind wood by zinc chloride using response surface methodology. *Bioresource technology*. 101(6), 1974–1982. doi: 10.1016/j.biortech.2009.10.031.

Salimi, M. N., Bridson, R. H., Grover, L. M., Leeke, G. A., 2012. Effect of processing conditions on the formation of hydroxyapatite nanoparticles. Powder Technology. 218, 109–118. doi:10.1016/j.powtec.2011.11.049

Sasikumar, S., Vijayaraghavan, R., 2006. Low Temperature Synthesis of Nanocrystalline Hydroxyapatite from Egg shells by Combustion Method. Trends in Biomaterials and Artificial Organs. 19, 70–73.

Srivastava, V. C., Mall, I. D., Mishra, I. M., 2008. Removal of cadmium (II) and zinc (II) metal ions from binary aqueous solution by rice husk ash. Colloids and Surfaces A: Physicochemical and Engineering Aspects. 312(2-3), 172–184.

Shrivastava, P. K., & Gupta, S. K. 2015. Removal of chromium from waste water by adsorption method using agricultural waste materials. *International Journal of Chemical Sciences and Applications*, 6, 1–5.

Tang, C., Zhang, R., Wen, S., Li, K., Zheng, X., & Zhu, M. 2009. Adsorption of Hexavalent Chromium from Aqueous Solution on Raw and Modified Activated Carbon. *Water Environment Research*, 81(7), 728–734.

Ulatowska, J., Stala, Ł., Polowczyk, I., 2021. Comparison of Cr (VI) Adsorption Using Synthetic Schwertmannite Obtained by Fe^{3+} Hydrolysis and Fe^{2+} Oxidation: Kinetics, Isotherms and Adsorption Mechanism. *International Journal of Molecular Sciences*. 22(15), 1–22. doi: 10.3390/ijms22158175.

WHO, 2017. Guidelines for Drinking-Water Quality, fourth ed., WHO, Press, Geneva.

Yakout, S. M., El-Deen, G. S., 2016. Characterization of activated carbon prepared by phosphoric acid activation of olive stones. *Arabian Journal of Chemistry*. 9, S1155–S1162. doi:10.1016/j.arabjc.2011.12.002

Zhang, X., Hao, Y., Wang, X., Chen, Z., 2017. Adsorption of iron (III), cobalt (II), and nickel (II) on activated carbon derived from Xanthoceras Sorbifolia Bunge hull: mechanisms, kinetics and influencing parameters. Water Science and Technology, 75(8), 1849–1861. doi: 10.2166/wst.2017.067.